Toehold length of target ssDNA affects its reaction-diffusion behavior in DNA-responsive DNA-co-acrylamide hydrogels.

Eleonóra Parelius Jonášová, Astrid Bjørkøy and Bjørn Torger Stokke.*

Biophysics and Medical Technology, Dept of Physics, NTNU - Norwegian University of Science and Technology, NO-7491 Trondheim, Norway.

responsive hydrogels, toehold, partitioning, DNA, acrylamide, strand displacement, interferometer, confocal laser scanning microscopy.

ABSTRACT In the present study we expand on the understanding of hydrogels with embedded deoxyribonucleic acid (DNA) crosslinks, from the overall swelling to characterization of processes that precede the swelling. The hydrogels respond to target DNA strands due to a toehold-mediated strand displacement reaction in which the target strand binds to and opens the dsDNA crosslink. The spatiotemporal evolution of the migrating target ssDNA was determined using confocal laser scanning microscopy (CLSM). The concentration profiles revealed diverse partitioning of the target DNA inside the hydrogel as compared to the immersing solution: excluding a non-binding DNA, while accumulating a binding target. The data show that longer toehold results in faster crosslink opening, but reduced diffusion of the target, thus resulting in only moderate increase in the overall swelling rate. The parameters obtained by fitting the data

using a reaction-diffusion model were discussed in view of molecular parameters of the target ssDNA and hydrogels.

Introduction

DNA and DNA-hybrid hydrogels are responsive hydrogels where the DNA in the hydrogel and its interactions with the components in immersing solution are key in transforming molecular changes to altered hydrogel state.[1–4] The unique appeal of incorporating DNA in a hydrogel is due to the high specificity of the complementary base pairing in hybridization reaction. The versatility and tunability lies in the combination of the large number of possible unique base pair sequences accessible by custom-design and high degree of control over the molecule's higher order structure and its interactions with other DNA molecules or other types of molecules through potential aptamer functionality.[5] The rapidly growing field of DNA nanotechnology is taking advantage of these properties that make DNA a unique building block.[6–11]

Conjugation of DNA within hydrogels allows translation of the specific and controllable interactions on molecular level to the micro- or even macro-level of the hydrogel. The level of control, specificity and versatility of DNA as a sensing moiety, paired with the hydrogels' tunability, biocompatibility and responsiveness at various length scales, underpin the potential of DNA-hybrid hydrogels' application within biosensing[12–21], diagnostics[22], targeted drug delivery[23–25] as well as cell culturing[26], scaffolds in tissue engineering[27,28] and various soft devices[29,30].

We have previously developed a sensor platform based on hydrogels integrated on an optical fiber for interferometric readout of changes in the optical length with 2 nm resolution for hydrogels with dimensions of about 50 μm.[31] This setup was used to study DNA-polyacrylamide

hydrogels applying a particular molecular design first reported by Nagahara and Matsuda[32] in 1996 that respond by swelling to the presence of a specific oligonucleotide.[33,34] The recognition is supported by partially double stranded DNA (dsDNA) crosslinks within the hydrogel that bind the target oligonucleotide, and subsequent toehold-mediated strand displacement. In this process, the invading single-stranded DNA (the target ssDNA) will hybridize with one of the strands (the sensing strand) in the DNA crosslink after binding to a complementary region called the toehold. By branch migration, a back and forth migration of the junction point where the three strands meet, the invading strand is displacing the complementary oligonucleotide in the DNA duplex called the blocking strand. Eventually, the blocking strand is completely displaced, and a more stable DNA duplex is formed. Completion of the strand displacement leads to dissociation of the dsDNA link between network strands, thus reducing the number of crosslinks and facilitating transformation of the processes at the molecular level to a (local) change in the swelling state. The overall swelling rates have been reported for various bp-lengths of complementary dsDNA regions as well as toehold regions for the target strands diffusing into the hydrogels.[34]

The interferometric readout platform provides high resolution information on the swelling of the hydrogels as a response to the diffusing target DNA as an average over the changes along the optical path, but it does not provide information on localized swelling. In the present work, we employ fluorescent labelling and confocal laser scanning microscopy (CLSM) to determine the spatiotemporal ssDNA target apparent diffusion through the gel, and how it is affected by the length of the toehold region. This approach provides insight into the cascading processes, starting by the attachment of invading ssDNA, the opening of a DNA crosslinks in the hydrogel, and ending with a change in the hydrogel volume. The target can be described as undergoing a reaction-diffusion process, where its net transport is the result of the interplay between its

diffusion inside the hydrogel and the binding and dissociation to and from the hydrogel-bound dsDNA. The translation mechanism of the change from the molecular DNA level to the hydrogel level determines the overall response time of the system and thus is of interest in most applications. A thorough understanding of the processes preceding the swelling is necessary in order to better design and tune the kinetics of the gel swelling to the needs of each application.

Materials and methods

Materials

Acrylamide ≥ 99% (Aam), N, N'-methylenebisacrylamide ≥ 99.5% (Bis), squalane oil, dimethyl sulfoxide (DMSO), 3-(trimethoxysilyl) propyl methacrylate 98%, 1-hydroxycyclohexyl phenyl ketone 99% (HCPK), 2-amino-2-hydroxymethyl-propane-1,3-diol (Tris) and 7-[4-(trifluoromethyl)coumarin]-acrylamide (Aam-coumarin) were purchased from Sigma-Aldrich; ethylenediaminetetraacetcic acid (EDTA) and sodium chloride (NaCl) were obtained from VWR. Single-stranded DNA oligonucleotides with custom specified bp sequence and functionalized with an acrydite group, both unlabeled and fluorescently labelled at specific bp, were obtained from Integrated DNA Technologies (IDT, Coralville, USA). All materials were used without further purification. De-ionized water with resistivity 18.2 MΩ cm (Millipore Milli-Q) was used throughout.

Hydrogel design

The quasi-hemispherical shaped hydrogels were prepared at the end of optical fibers to support the interferometric length measurement.[31] The responsive hydrogels consist of a covalently crosslinked polyacrylamide network (10 wt% acrylamide, 0.6 mol% Bis) with additional partially double-stranded DNA crosslinks (0.2 mol%) (Figure 1). In addition, pure

polyacrylamide hydrogels PolyAam08 without DNA, but with crosslinking density equivalent to that of DNA-hydrogels (0.8 mol% Bis), were prepared.

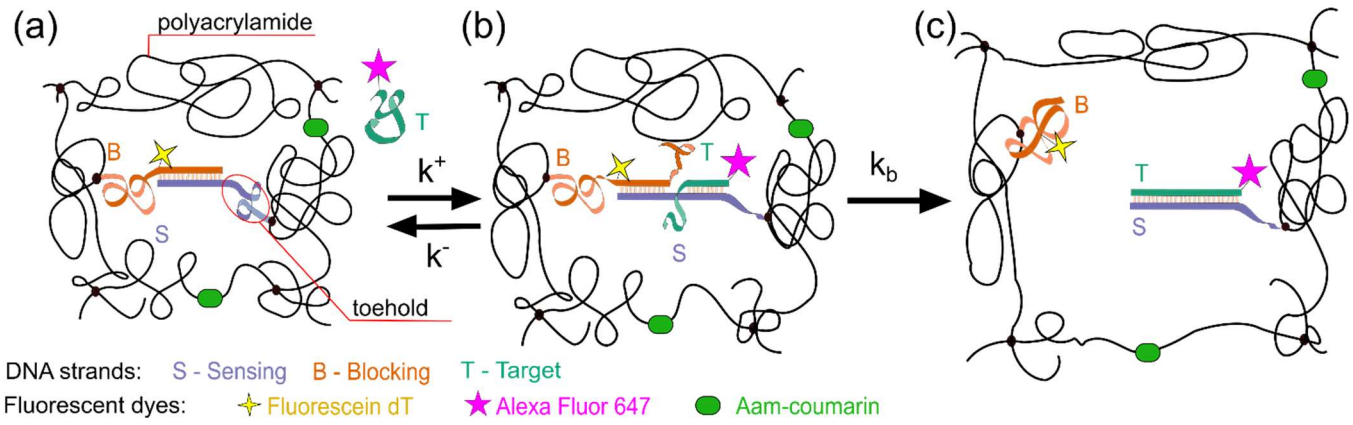

Figure 1 Schematic illustration of the DNA-polyacrylamide hydrogel network and the process of toehold-mediated strand displacement. The target DNA (T) binds to (rate constant k^+) and dissociates (rate constant k^-) from the hybridized sensing-blocking SB dsDNA in the hydrogels (Figures 1a, 1b), and a bound target DNA undergoes branch migration with a rate k_b to dissociate the SB duplex (Figures 1b, 1c). Three different types of gels were prepared: SB hydrogels with no dyes attached to the network or network-bound DNA, CoumSB hydrogels containing only Aam-coumarin and SBF hydrogels only labeled with Fluorescein dT on B strand.

The hybridized sensing strand (S) and blocking strand (B) are covalently attached to the network, forming the dsDNA crosslinks. S and B oligonucleotides were obtained with an acrydite group at 5'-ends to allow covalent bonding with the polyacrylamide network. The S and B strands were designed with 20 bases with a 10-base complementary region at their 3' ends which is referred to as the blocking region (Figure 2). The hybridized regions were designed with a high GC content to ensure a melting temperature above the ambient temperature of 22°C used

in the experiments. The melting temperature of the SB duplex was estimated to 48.9°C using online oligonucleotide properties calculator OligoCalc.[35]

The DNA crosslink can be opened by a target T strand in a toehold-mediated strand displacement process (Figure 1, 3).

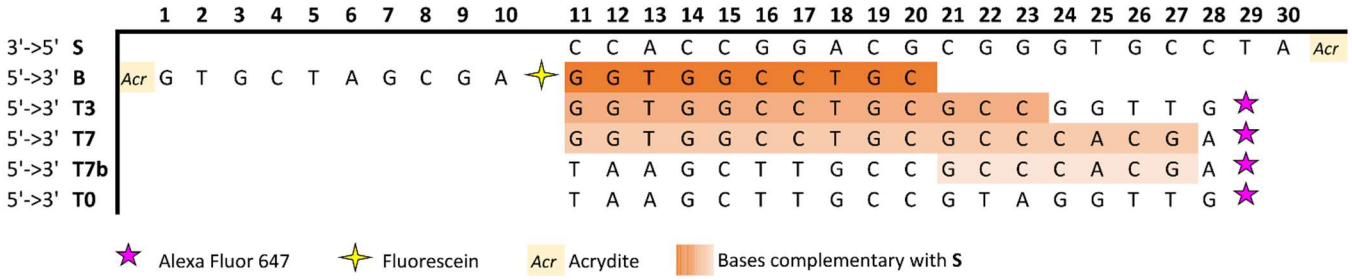

Figure 2 DNA sequences of the sensing S, blocking B and target strands T0, T3, T7 and T7b. The positions of the fluorescent dyes and the acrydite groups are shown, and the complementary regions between S and B, and S and the targets are highlighted.

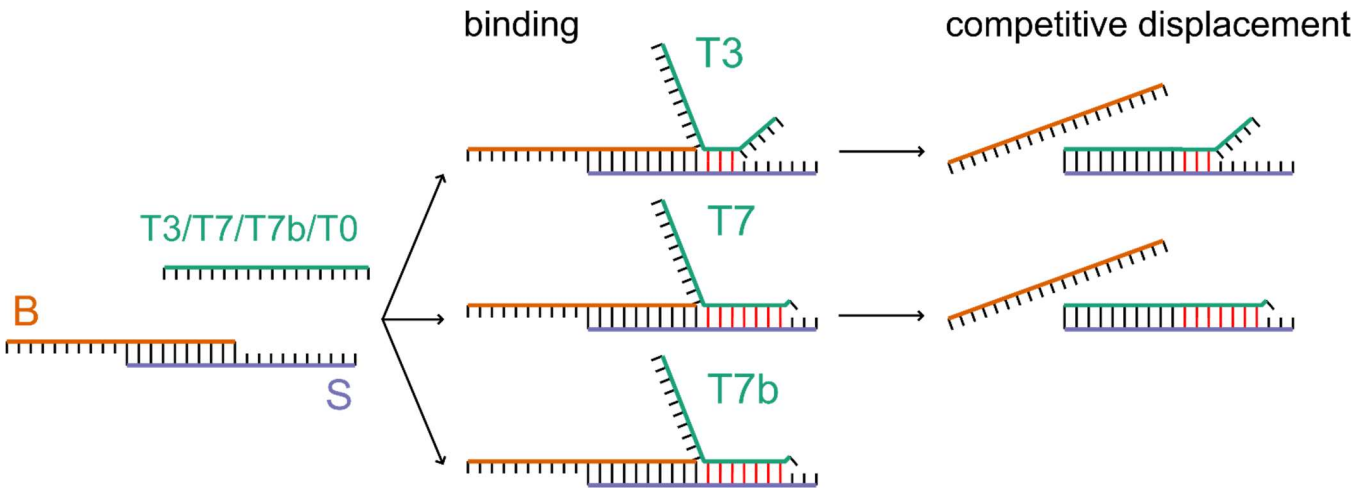

Figure 3 Schematics of the interactions (binding and competitive toehold-mediated strand displacement) between the dsDNA crosslink SB and various target strands T3, T7, T7b and T0. The bonds in the complementary region of the toeholds are shown in red.

The hydrogels were immersed in aqueous buffer solutions of 20 μM target ssDNA of either of the targets T0, T3, T7 or T7b (each consisting of 18 bases) (Figure 2 and 3). T3 and T7 strands

are complementary to the sensing strand S for the same bases as B (the blocking region), as well as an additional complementary region (toehold) of 3 and 7 bases respectively, while T7b is only complementary to S on a toehold region of 7 bases. T0 is designed to be non-complementary to S and does not bind.

Labelling strategy

Fluorescent dyes were used to monitor the processes taking place before and during the swelling of the hydrogel. The hydrogels were immersed in aqueous buffer solutions with target ssDNA (T0, T3, T7 or T7b) where 10% of the target ssDNA were labelled with Alexa Fluor 647 at their 3' ends to be used as a reporting molecule when visualizing their diffusion and binding within the hydrogel.

In addition to fluorescent labelling of the target strands, several strategies involving labelling of the hydrogel (polyacrylamide or hydrogel-bound DNA) were explored with the intention of using this as internal reference or to gain more understanding of the underlying molecular processes. While these strategies were not successful (SI: Use of FRET for monitoring of crosslink opening, Figure S1 and S2), we included information on the labelled hydrogels alongside the unlabeled ones to report on the observed effects of fluorescent dye incorporation.

Three different types of hydrogels with respect to presence of fluorescent dyes were prepared. Hydrogels denoted SB carried no fluorescent dyes; CoumSB hydrogels included a coumarin-labeled acrylamide incorporated in the polymer network (at concentration 0.05 mol% of acrylamide monomer); and SBF hydrogels had 10% of the blocking strands labelled with Fluorescein dT.

Pregel and target DNA solutions

Pregel solutions were prepared by dissolving 10 wt% Aam, (optionally also including 0.05 mol% Aam-coumarin), 0.6 mol% Bis, 0.2 mol % dsDNA (SB) and 0.13 mol% HCPK in buffer (10 mM Tris, 1 mM EDTA and 150 mM NaCl, adjusted to pH 7.5). HCPK and Aam-coumarin were first dissolved in DMSO to the concentrations of 0.1 M and 0.11 M respectively, before being added to the pregel solution. SBF hydrogels were prepared with 10 % of the B oligonucleotides labelled with Fluorescein dT. After preparing the pregel solution, a minimum of 3 hours of passive mixing was allowed, to ensure the formation of SB duplexes. PolyAam08 hydrogels were prepared without DNA, but with 10 wt% Aam and 0.8 mol% Bis, i.e. identical total crosslinker density to the DNA hydrogels (where both Bis and DNA serve as crosslinkers).

Stock solutions of target ssDNA were prepared by dissolving the T0, T3, T7 or T7b strands in aqueous buffer (10 mM Tris, 1 mM EDTA and 150 mM NaCl, adjusted to pH 7.5) to a concentration of 60 µM and kept at -18°C. The target stock solutions were prepared with 10% Alexa Fluor 647 labelled target oligonucleotides.

All solutions were stored at -18°C.

Fiber preparation

The optical fibers (SMF-28-J9 from ThorLabs, diameter without coating 125 µm) were first stripped of the coating and the ends were cut to obtain a flat and even surface (cutter: Fitel model S323, Furukawa Electric Co. Ltd.). After cleaning with ethanol, the ends were treated with 0.1 M HCl solution for 20 minutes and cleaned with ethanol again. Then the fiber ends were soaked for 15 minutes in a 2 vol% solution of 3-(Trimethoxysilyl) propyl methacrylate dissolved in degassed MiliQ water at pH 3.5. The methacrylated fibers were again cleaned with ethanol and with duct tape to remove dust from the end face. The silanization procedure resulted in surface-bound methacrylate groups to ensure covalent linking of the acrylamide during polymerization.

Gel preparation

A small amount of the pregel solution (~ 0.3 nL) was deposited at the end face of an optical fiber immersed in a squalane oil droplet and polymerized using UV-light. The squalane oil was saturated with HCPK (2.6 mg/mL). The oil solution was prepared at least 2 hours before polymerization, kept in the dark and on constant stirring and used for up to 1 week.

A small aliquot of the pregel solution was manually deposited on the end of the optical fiber using a pipette as aided by inspection through a stereo microscope. Polymerization was initiated using UV light from a UV lamp (Fiber coupled LED UV source M340F3, nominal wavelength 340 nm, ThorLabs, or Dymax blue wave, 50W) for 5 minutes.

Interferometry

The end of the fiber with the hydrogel was inserted into an Eppendorf tube containing 200 µL of buffer solution (10 mM Tris, 1 mM EDTA and 150 mM NaCl, adjusted to pH 7.5) and left to equilibrate for at least an hour. 100 µL of the stock target solution (60 µM target DNA) was then added to obtain the final target solution (20 µM target DNA, of which 10% fluorescently labeled, pH 7.5, 150 mM NaCl). The monitoring of the total gel length along the axis and its changes was performed using the interferometric setup, described in detail elsewhere.[31] Briefly, a light wave (wavelength range 1530-1560 nm) is sent through the fiber and along the axis of the hydrogel and light reflected from the fiber-hydrogel and hydrogel-solution interfaces is detected. The gel is a micro Fabry-Perot cavity and the physical length of the hydrogel R (precision 1 µm) is determined by the free spectral range of the cavity. The phase change of the interference signal is used to determine changes in the length of the hydrogel ΔR due to changes in the swelling (precision 2 nm). The data logging started 90 seconds prior to the addition of target strands. The data was recorded every second for up to 150 minutes.

Using the initial size $R_0 = R(t = 0)$, (t = 0 referring to addition of target stock solution to the immersing aqueous buffer) and the change in size of the hydrogel ΔR, relative swelling was calculated:

$$\mathrm{R\%} = \Delta R / R_0. \qquad 1$$

Confocal Laser Scanning Microscopy

The end of the fiber with the covalently attached hydrogel was pinched of using tweezers and glued to the bottom of a Glass Bottom Microwell Dish (P35G-1.5-10-C) from MatTek. 200 µL of the buffer solution (10 mM Tris, 1 mM EDTA and 150 mM NaCl, adjusted to pH 7.5) was then added, and the gel was left to equilibrate for at least 1 hour before the addition of the target stock solution.

The final target solutions (20 µM target DNA, with 10% fluorescently labeled strands, pH 7.5 and 150 mM NaCl) were prepared immediately prior to CLSM time lapse imaging by adding 100 µL of target stock solutions (60 µM target DNA) to the buffer solution equilibrating the gel. Time lapse imaging of the gels was performed at 22°C using a Confocal Laser Scanning Microscope (Zeiss LSM800) with a 40x, NA=1.2 water immersion objective (optical slice thickness of 0.9 µm). The imaging started 30-40 seconds after adding the stock target solution and a micrograph was acquired every 60 sec for up to 4 hours. The excitation wavelengths were 640 nm, 488 nm and 405 nm for Alexa Fluor 647, Fluorescein dT and Aam-coumarin, respectively. Bandpass filters of 650-700 nm, 500-550 nm and 400-600 nm were employed on the emission side to capture the fluorescence from Alexa Fluor 647, Fluorescein dT and Aam-coumarin respectively.

Acquiring fluorescence intensity profiles from CLSM micrographs

Custom scripts in Matlab R2017a (Mathworks) were developed for analysis and visualization of fluorescence intensity from the time lapse CLSM micrographs. Fluorescence intensity profiles

were first extracted from the DNA hydrogel micrographs over several lines and averaged (Figure 4 showing a representative hydrogel of length 60µm). The profiles used as basis for the averaging were acquired from a micrograph in a plane parallel to the coverglass and the fiber axis (core) (shown in red in Figure 4a). Averaged intensity profiles were extracted from a circular sector with a central angle of 20°. A profile was acquired every half a degree (Figure 4c). A plane rather than a cone was chosen for practical reasons and because of possible depth-dependent loss of fluorescence due to absorption and refraction. The averaging procedure assumes a spherical geometry; however, the hydrogels are not perfectly spherical. To minimize the resulting error, the averaging angle was restricted to 20°.

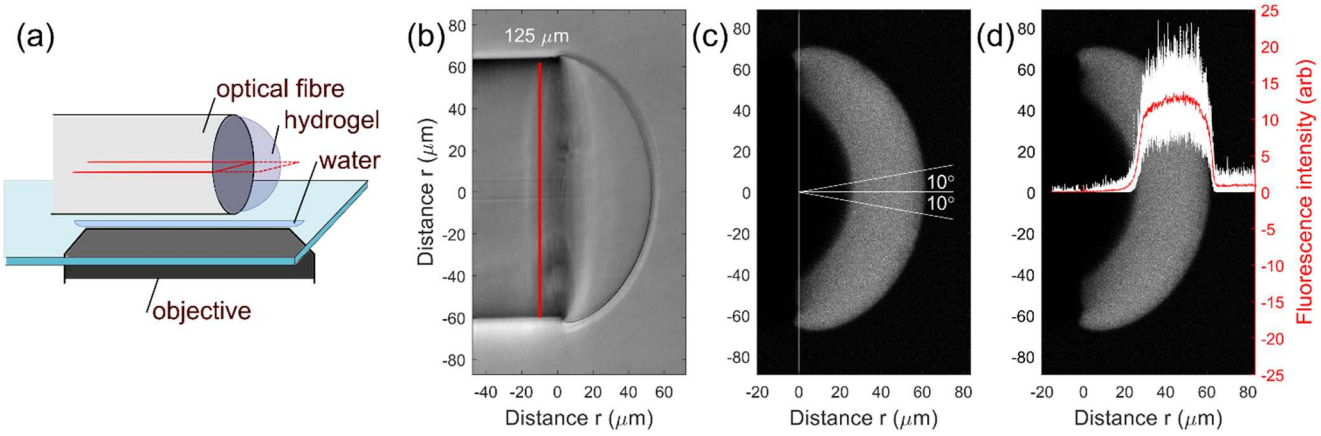

Figure 4 Acquiring intensity profiles from confocal micrographs. a) Schematics of an optical fiber with a hydrogel attached to its end face as it is imaged using confocal laser scanning microscopy. Fluorescence micrographs were acquired at a plane through the middle of the hydrogel, at a 62 µm depth, shown in red. b) Transmitted light image of a hydrogel and the fiber end face. c) Micrograph showing the fluorescence acquired from Alexa Fluor 647 on target strand T7. The image is showing an intermediate state during the swelling and is acquired 35

minutes after gel being immersed in the target solution. The distribution of target T7 in the particular gel reached equilibrium at 70 minutes. The lines depict the angle within which intensity profiles are extracted. d) The extracted individual fluorescence profiles from c) are shown in white and their average in red overlayed the fluorescence micrograph of the hydrogel. The fiber end face is located at $r = 0$.

Relationship between measured fluorescence intensity and concentration

Partitioning of non-binding oligonucleotide T0 in DNA-hydrogels

The partition coefficient K_i of a solute i is defined as a ratio of its concentration in the gel c_{gel} and in the solution c_{sol} at equilibrium:

$$K_i = \frac{C_{gel}}{C_{sol}} \qquad 2$$

This partitioning is governed by equal chemical potential of the solute in the two phases. In addition to size effects, the partitioning is dependent on interactions between the hydrogel and the solute and thus is influenced by the properties of both. If these interactions are independent, they can be separated into individual contributions to the partition coefficient: [36]

$$lnK_i = lnK_{i,el} + lnK_{i,hphob} + lnK_{i,biosp} + lnK_{i,size} + lnK_{i,conf} + lnK_{i,o} \qquad 3$$

where *el*, *hphob*, *biosp, size*, *conf* and *o* denote, respectively, electrostatic, hydrophobic, biospecific affinity, size-related, conformational effects and other interactions.

Fluorescence intensity in the proximity of the fiber

Estimates of relative concentrations of the target T ($I_{TX/T0}$), X = 3 or 7, from the experimentally determined fluorescence intensity were obtained considering the effect of optical aberrations due to refraction caused by the presence of a glass fiber in the near vicinity of the hydrogel.[37] Previously, the loss of fluorescence due to the fiber was observed to extend up to

approximately 50 μm from the end face of the fiber into the solution.[37] Assuming this is unchanged by the presence of the hydrogel, the ratio between the fluorescence intensity inside the hydrogel 60 μm from the end of the fiber and the fluorescence intensity of the surrounding solution reflects the ratio of the target concentrations in these domains.

The fluorescence intensity inside the hydrogel can also be reduced due to increased absorption as well as refractive index difference between the hydrogel and the immersing solution used during microscopic imaging. However, we observed a corresponding decrease in fluorescence inside the gel compared to the solution also when imaging in a plane closer to the coverglass, suggesting no significant effect from absorption and refractive index mismatch, which means that the decrease in fluorescence is mostly due to partitioning and presence of the fiber.

Based on these assumptions, we used the ratio between the intensity inside the hydrogel at 60 μm from the end face and in the surrounding solution as the partitioning coefficient, i.e. assuming that the ratio of fluorescence intensities of the target DNA in the solution and in the hydrogel at 60 μm from the fiber reflects the ratio of the corresponding concentrations.

The shape of the intensity profiles within the hydrogel is distorted due to aforementioned presence of the glass fiber and does not reflect a real decrease in concentration in the vicinity of the fiber. This was corrected for by using a reference profile that was obtained by immersing the hydrogel in a solution of a non-binding target T0.[37] The averaged intensity (I_{TX}) profiles to be corrected were smoothed using a Savitzky-Golay filter, normalized so that the intensity of the surrounding solution is 1 and divided by smoothed and normalized (to maximum intensity in hydrogel being 1) reference profiles (Figure 5).

The alternative correction method employing Aam-coumarin as an internal reference yielded relative concentration profiles similarly resembling a more appropriate distribution (Figure S1).

However, the correction based on Aam-coumarin was not employed further due to a possible effect of the coumarin dye on the partitioning of the target DNA (see below) and due to observed dye-clustering.

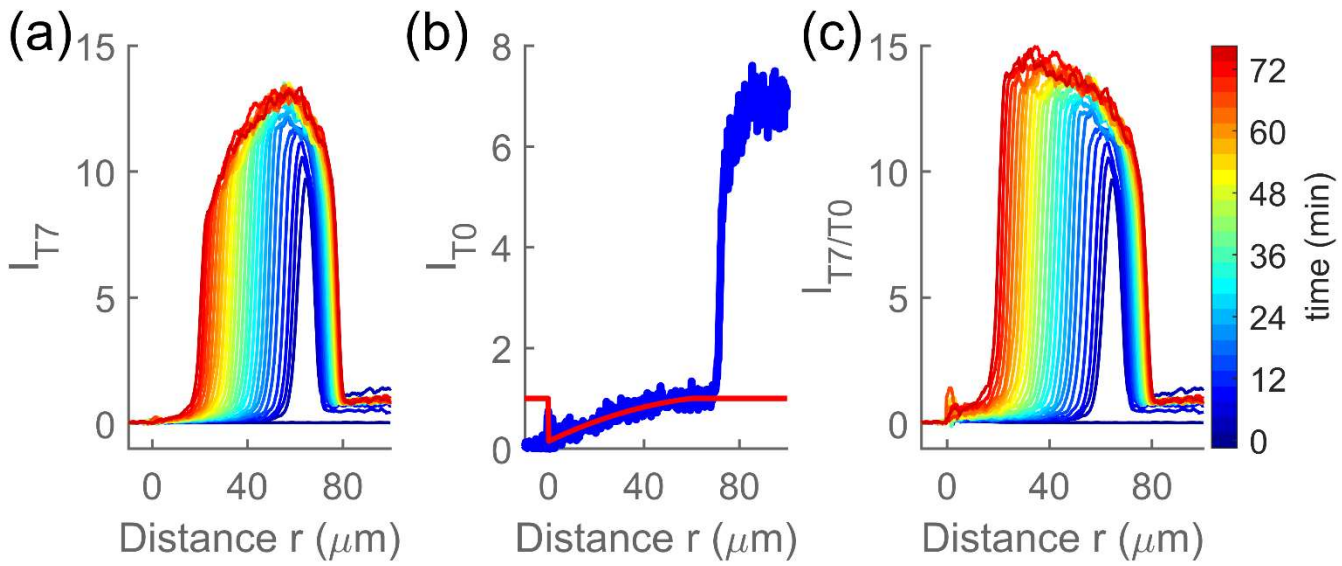

Figure 5 Correcting the intensity profiles for the optical effect caused by the presence of the fiber. a) Profiles showing the fluorescence intensity acquired from Alexa Fluor 647 attached to T7 strand (I_{T7}), smoothed and normalized such that the intensity of the fluorescence of the free solution is 1. A profile is shown for every 3rd minute after addition of the target to the immersing solution. The colorbar specifies for each profile its time point after addition of the target. b) In blue, equilibrium intensity profile of the non-binding target T0 (I_{T0}) inside (*r* less than 70 µm) and outside a hydrogel, smoothed and normalized so that the maximum intensity within the hydrogel is 1. In red, a second-degree polynomial fit to the part of the profile within the hydrogel. c) Intensity profiles I_{T7} from a) divided by a reference profile acquired from T0 (as shown in red in b)) to obtain the corrected relative intensity, i.e. estimated relative concentration $I_{T7/T0}$. The fiber end face is located at $r = 0$.

Parameter estimation of the spatiotemporal profiles

Finally, the relative concentration profiles $I_{TX/T0}$ were fitted to an error function to obtain empirical parameters reflecting the spatiotemporal evolution of the target DNA concentration profiles in the hydrogels. An error function was chosen as this is derived from a diffusion process and in the present case was found to fit the observed transitions in concentration (in the following referred to as wavefront). Only the parts of the profiles that were inside the gel, the wave propagating towards the fiber end face, were used for the fitting (Figure 6). The fitting function has the following form:

$$F(r) = A\,\mathrm{erf}\left(\frac{r - r_0}{\sigma\sqrt{2}}\right) + C \qquad 4$$

where r is the distance from the fiber end face along the axis of the hydrogel, A is half of the height of the wavefront, C is the height of the wavefront midpoint above 0, r_0 is the distance from fiber end face to the wavefront midpoint and σ relates to the width of the wavefront. Erf denotes a standard error function of the form

$$erf(x) = \frac{2}{\sqrt{\pi}}\int_0^x e^{-t^2}dt. \qquad 5$$

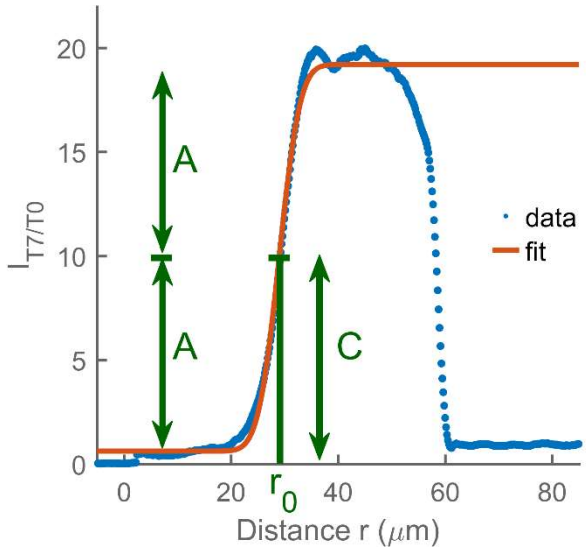

Figure 6 Fitting of the experimental concentration wavefront that is propagating towards the fiber end face to an error function (fiber end face at r = 0). Relative concentration profile $I_{T7/T0}$ normalized to the intensity of the surrounding solution (blue curve) along with the fit to error function (red curve).

The fitted function was also differentiated analytically at the wavefront midpoint $r = r_0$ to obtain the value of the steepest slope, reflecting the largest concentration gradient of the target T migrating into the hydrogel. This parameter was calculated as:

$$\left.\frac{dI_{T/T0}}{dr}\right|_{r=r_0} = \left.\frac{dF(r)}{dr}\right|_{r=r_0} = \frac{\sqrt{2}A}{\sqrt{\pi}\sigma} \qquad 6$$

The size *R(t)* of the hydrogel at each time was also determined by finding the location of maximal negative slope of each profile. For this purpose, experimental profiles were numerically differentiated.

From the fitting coefficients and measured size *R(t)* of the hydrogel, we obtained the relative transport of the targets T determined by the movement of the wavefront midpoint position into the hydrogel, $r_0\%\ (t)$

$$r_0\%\,(t) = \frac{R_0 - r_0}{R_0}, \qquad 7$$

to describe how far into the hydrogel the midpoint of target T is located at a given time.

Mathematical model for reaction-diffusion process of target T into the hydrogel

The concentration c of a molecule undergoing pure diffusion follows the Fick's second law, which reads

$$\frac{\partial c}{\partial t} = D\Delta c \qquad 8$$

where D is the diffusion coefficient, t is time and Δ is a Laplacian ($\Delta c = \sum_i \frac{\partial^2}{\partial x_i^2}$ with x_i being Cartesian coordinates).

For diffusion within a radially symmetric sphere the concentration $c(\hat{r}, t)$ as a function of time t and relative radial position $\hat{r} = r/R$ (where r is the radial position and R the radius of the sphere) is given as:[38]

$$\frac{\partial c}{\partial t} = \frac{1}{\hat{r}^2}\frac{\partial}{\partial \hat{r}}\left(\hat{r}^2 \frac{D}{R^2}\frac{\partial c}{\partial \hat{r}}\right) \qquad 9$$

We assume that the equations valid for diffusion in a sphere are also valid for diffusion along the axis of a half sphere, as is our case. The hard boundary at the fiber end causes reflection of the diffusing molecules with similar result as diffusion from the other (missing) half of the sphere would have given. The hydrogels in question are also not perfectly hemispherical, which will introduce error into the model, depending on the magnitude of the deviation from a spherical geometry.

The reaction of strand T with the SB duplex integrated in the hydrogel can be modeled as a two-step process.[39] In the first step, T binds to the toehold region of S, creating a three-strand complex SBT. The junction point then migrates until eventually reaching the other end of the S-T binding region and dissociating into a strand B and ST duplex. The reaction rate constant for

the hybridization of the toehold is denoted k^+, the reaction rate for its dissociation k^-. The rate constant for the branch migration process of a bound target is denoted k_b (see also Figure 1). When the crosslink is opened, we assume the reverse reaction is negligible, since the opening of the crosslink will lead to network relaxation and the hydrogel-bound strands S and B can be expected to be too far from each other for the rebinding to occur.[40] The evolution of the concentration of the target T can then be described by the following partial differential equations (PDEs):

$$\frac{\partial c}{\partial t} = \frac{1}{\hat{r}^2}\frac{\partial}{\partial \hat{r}}\left(\hat{r}^2 \frac{D}{R^2}\frac{\partial c}{\partial \hat{r}}\right) - k^+ c m_f + k^- m_c \quad 10$$

$$\frac{\partial m_c}{\partial t} = k^+ c m_f - k^- m_c - k_b m_c \quad 11$$

$$\frac{\partial m_o}{\partial t} = k_b m_c \quad 12$$

$$m_t = m_f + m_c + m_o \quad 13$$

where c is the molar concentration of the free target T, m_t is the total molar concentration of accessible binding cites, m_f is the molar concentration of free binding sites, m_c the molar concentration of three-strand complexes and m_o of the open crosslinks. Equation (13) is the conservation of binding sites in the various possible states.

By introducing $\alpha = \frac{D}{R^2} > 0$, equation 10 can be rewritten as:

$$\frac{\partial c}{\partial t} = \frac{\alpha}{\hat{r}^2}\frac{\partial}{\partial \hat{r}}\left(\hat{r}^2 \frac{\partial c}{\partial \hat{r}}\right) - k^+ c m_f + k^- m_c \quad 14$$

By expressing m_f as a function of m_c, m_o and m_t we obtain a set of three equations (for c, m_c and m_o) with their corresponding boundary (B.C.) and initial conditions (I.C.):

$$\frac{\partial c}{\partial t} = \frac{\alpha}{\hat{r}^2}\frac{\partial}{\partial \hat{r}}\left(\hat{r}^2\frac{\partial c}{\partial \hat{r}}\right) - k^+ cm_t + k^+ cm_c + k^+ cm_o + k^- m_c \quad 15$$

$$B.C.: \frac{\partial c(0,t)}{\partial \hat{r}} = 0, \quad t \geq 0 \quad 16$$

$$c(1,t) = c_{out} \quad 17$$

$$I.C.: c(\hat{r},0) = \begin{cases} 0, & 0 \leq \hat{r} < 1 \\ c_{out}, & \hat{r} = 1 \end{cases} \quad 18$$

$$\frac{\partial m_c}{\partial t} = k^+ cm_t - k^+ cm_c - k^+ cm_o - k^- m_c - k_b m_c \quad 19$$

$$B.C.: \frac{\partial m_c(0,t)}{\partial t} = 0 \quad 20$$

$$m_c(1,t) = 0 \quad 21$$

$$I.C.: m_c(\hat{r},0) = 0, \quad 0 \leq \hat{r} \leq 1 \quad 22$$

$$\frac{\partial m_o}{\partial t} = k_b m_c \quad 23$$

$$B.C.: \frac{\partial m_o(0,t)}{\partial t} = 0 \quad 24$$

$$m_o(1,t) = 0 \quad 25$$

$$I.C.: m_o(\hat{r},0) = 0, \quad 0 \leq \hat{r} \leq 1 \quad 26$$

where c_{out} is the concentration at the boundary of the hydrogel.

Numerical solution of the reaction-diffusion PDEs

To solve this system of equations numerically, we can apply the method of lines which reduces the PDE to a system of ordinary differential equations (ODEs) by discretizing one dimension (here the radial dimension) onto a finite grid with equal spacing and coordinates $\hat{r}_i = i\Delta\hat{r}$ for i=0,1,...,N. Similarly, c, m_o, m_c at grid point i will be denoted as c_i, m_{oi} and m_{ci}, respectively. The spatial derivatives are approximated using the second order centered finite difference

approximation in spherical coordinates[41] and a system of ordinary differential equations (ODEs) is obtained at each point in the grid:

$$\frac{dc_i}{dt} = \begin{cases} \frac{6\alpha}{\Delta\hat{r}^2}(c_1 - c_0) - k^+c_0m_t + k^+c_0m_{c0} + k^+c_0m_{o0} + k^-m_{c0}, & \text{if } i = 0; \\ 0, & \text{if } i = N; \\ \frac{\alpha}{i\Delta\hat{r}^2}[(i+1)c_{i+1} - 2ic_i + (i-1)c_{i-1}] - k^+c_im_t + k^+c_im_{ci} + k^+c_im_{oi} + k^-m_{ci}, & \text{otherwise} \end{cases} \quad 27$$

$$\frac{dc_{bi}}{dt} = \begin{cases} 0, & \text{if } i = N; \\ k^+c_im_t - k^+c_im_{ci} - k^+c_im_{oi} - k^-m_{ci} - k_bm_{ci}, & \text{otherwise} \end{cases} \quad 28$$

$$\frac{dc_{oi}}{dt} = \begin{cases} 0, & \text{if } i = N; \\ k_bm_{ci}, & \text{otherwise} \end{cases} \quad 29$$

This set of equations can be solved using MATLAB built in ODE solver functions, here *ode15s*.

Fitting the model to experimental data

The mathematical model of the reaction-diffusion process in a sphere was then fitted to the experimental data using MATLAB's *fminsearch* function. The boundary conditions for the free target concentration *c* were chosen with the partitioning effect taken into account for each of the different types of the hydrogels, i.e., the concentration of the free target at the boundary was $c(\hat{r} = 1, t) = c_{out} = K\,c_{sol}$, where K is the partition coefficient of nonbinding target T0 for the given type of gel and c_{sol} is the target concentration in the immersing solution. The experimentally determined values of K were employed in the modelling.

The model does not account for swelling and the experimental data used for the fitting were comprised of parts of the profile that fall within the hydrogel's initial size, i.e. the length of the hydrogel used in the modelling was constant equal to its initial length R_o.

We also excluded several profiles at the beginning and end of the experiment, as the profiles were getting established and as they reached the fiber end face.

The parameters α, k^+, k^-, k_b, m_t and t_{delay} were determined in the fitting procedure. The first scan was performed 20-40 seconds after adding the target stock solution in the physical experiments. The parameter t_{delay} was added to the model accounting for this time-shift, and the parameter estimation also included fitting of parameter values for t_{delay}.

Results and discussion

Partitioning

The normalized fluorescence intensity profile of non-binding T0 target DNA labeled with Alexa Fluor 647 throughout various hydrogels after equilibration were determined for SB, CoumSB, SBF hydrogels as well as pure polyacrylamide hydrogels PolyAam08 (Figure 7a). These profiles clearly indicate exclusion of T0 DNA from the hydrogels, and the data from the individually prepared hydrogels clearly indicate that the extend of exclusion also depends on the nature of the hydrogel.

The partitioning coefficient was calculated as the ratio between the fluorescence intensity inside the hydrogel and the fluorescence intensity of the surrounding solution and averaged for hydrogels of the same type. The intensity inside the hydrogel was measured at a distance greater than 60 μm from the fiber, in order to avoid the effect of refraction from the fiber. The measured partition coefficients are depicted in Figure 7b. The partitioning of a binding target (T7) at equilibrium was also compared to the partitioning of a nonbinding target (T0) inside the same hydrogel (Figure 7c).

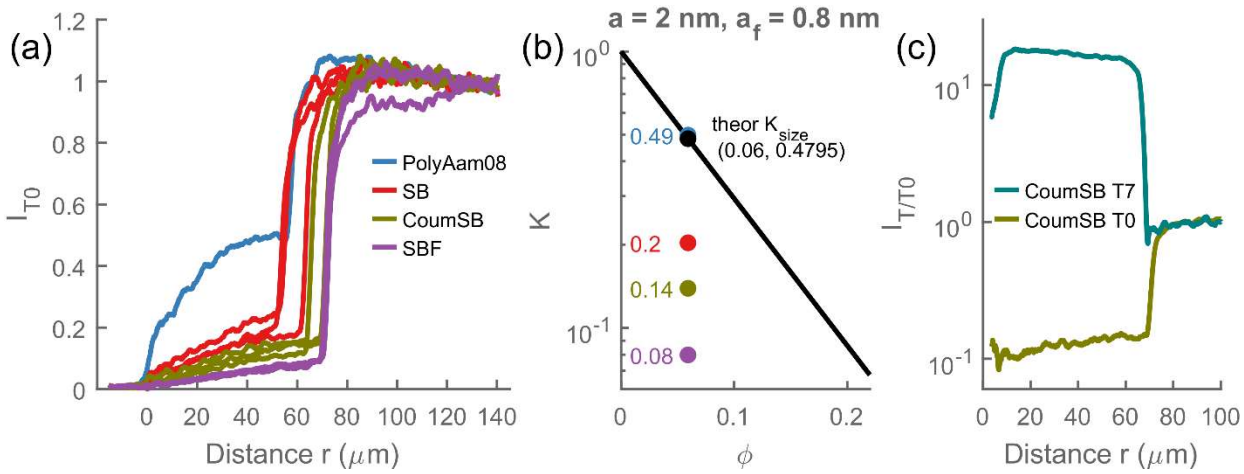

Figure 7 a) Normalized fluorescence intensity of non-binding T0 target labelled with Alexa Fluor 647 in different hydrogels: SB, CoumSB, SBF and PolyAam08. b) Plot of partition coefficient K_{size} as a function of matrix volume fraction ϕ according to theory of Ogston (continuous line). The points depict the experimentally determined K of the T0 target DNA for the hydrogels shown in a). c) Relative concentration profiles of the non-binding target T0 and in binding target T7 in the same CoumSB hydrogel at equilibrium. Fiber end face at $r = 0$.

Several of the interactions that affect the partitioning (equation (3)) can be expected to occur in the case of the target DNA strands in the DNA-hydrogels studied here. Size effects are a result of physical properties of the system, such as the size and shape of the solute and the size and shape of the hydrogel pores. Even when the solute is not physically obstructed from entering the gel network (due to size larger than the pore size), lower entropy due to fewer orientations available within the hydrogel contribute to exclusion of the solute.[36] Since PolyAam08 hydrogels do not contain DNA crosslinks and the polyacrylamide network is itself electrically neutral, there are no electrostatic or biospecific interactions and the contribution to the total partition coefficient are expected to arise from size effects. Ogston[42] provided an equation to estimate the size contribution K_{size} to the partitioning coefficient K. It is based on placing spheres of radius a (solute) in a matrix of long cylindrical fibers of radius a_f, with a total volume fraction ϕ:

$$K = e^{-\phi\left(1+\frac{a}{a_f}\right)^2} \quad (30)$$

Approximating the parameter a by the radius of gyration of a single stranded DNA of 20 base pairs (a = 2 nm)[43] and using experimentally determined volume fraction $\phi = 0.06$, and fiber radius $a_f = 0.8$ nm from Williams at al[44], we would expect the size contribution to the partitioning coefficient to be $K_{size} = 0.48$ (Figure 7b).

There is excellent agreement between the theoretical value of K_{size} and the experimentally observed one for T0 DNA within the polyacrylamide hydrogels without any added DNA (PolyAam08) (Figure 7b). This also indicates that the ratio of the fluorescence intensity in the outermost layer of the hydrogel (over 60 μm from the fiber) compared to the surrounding solution reflects the actual ratio of the concentrations, unaffected by the presence of the fiber and/or distorted by other phenomena, such as increased light absorption inside the hydrogel.

There is a clear effect on the partition coefficient of T0 DNA due to the presence of hydrogel-bound DNA, e.g., difference observed for SB hydrogel as compared to PolyAam08 (Figure 7a). Note that the PolyAam08 and the DNA-crosslinked hydrogels (SB, CoumSB and SBF) were all prepared with the same 0.8 mol% crosslinker concentration relative to the Aam monomer, with only Bis or Bis and dsDNA mediated crosslinks, respectively. The fact that DNA is a polyanion, electrostatic interactions will be present between the hydrogel-bound DNA (S and B) and the solute (target T), favoring exclusion of T from the hydrogel in such a case (Figure 7a). The presence of the fluorescent dyes also influences the partition coefficient, as indicated from the data from CoumSB and SBF hydrogels (Figure 7a and b). This could be through effects on the stiffness of the chains, changes in hydrophobicity or charge. In particular, the hydrophobic character of fluorescein and coumarin and their difference in this, as indicated by their aqueous solubility (0.01 M for coumarin[45], 1.5 x 10^{-4} M for fluorescein[46]), or the decrease in solution

critical temperature of poly(N-isopropylacrylamide) hydrogels upon integration in these,[47] suggests that their hydrophobicity has a possible effect on the partitioning, e.g. differences in $K_{i,hphob}$ in eq. 3.

For DNA-hydrogels immersed in solutions containing targets T that bind to the DNA incorporated in the hydrogel, this biospecific affinity leads to accumulation of the solute T inside of the hydrogel and a partition coefficient greater than 1. In Figure 7c, the effect of biospecific affinity on the partitioning can be seen, since the only difference between targets T7 and T0 is their complementarity, or lack thereof, with the hydrogel-bound DNA. The target T7 binds to the network and accumulates within the hydrogel, reaching concentrations larger than the concentration of the surrounding solution by one order of magnitude. The observation reported in Figure 7c indicates that the biospecific contribution to the partitioning (Eq. 3) is approximately 2 orders of magnitude greater as compared to the exclusion effects (T7 probe as compared to T0).

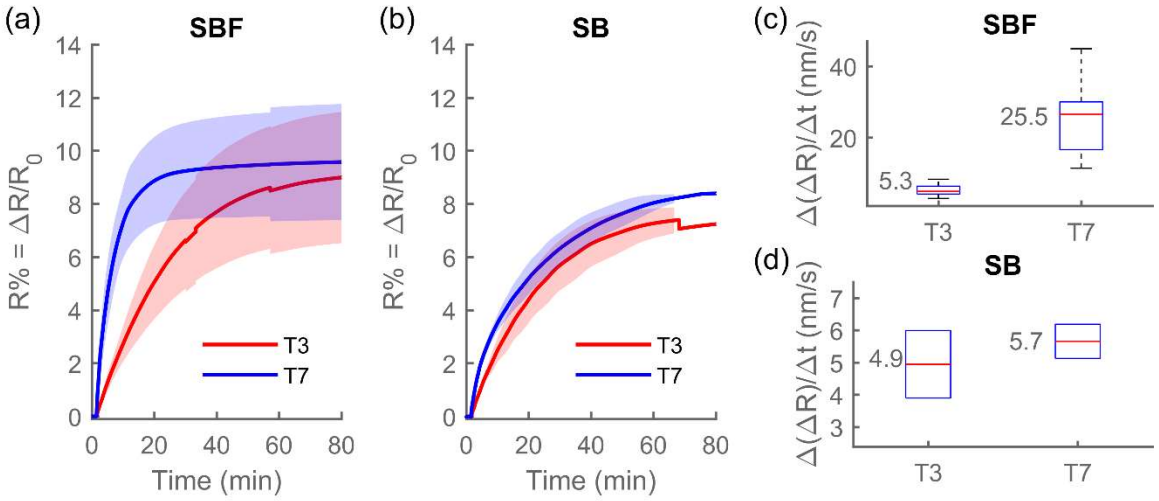

Figure 8 Relative swelling kinetics as determined by interferometry of SBF (a) and SB (b) hydrogels immersed in aqueous buffer solutions following an addition of either T7 or T3 to the

immersing solution to a concentration of 20 μM. The lines show the average values and the shaded areas the standard deviation of several independent experiments (13 for SBF-T7, 7 for SBF-T3, and 2 for SB). The discontinuities in the curve are due to different time durations of some of the experiments. All individual curves are in Figure S9. Figures (c) and (d) show the initial rate of swelling at $t = 0$ as box plots.

Effect of toehold length on the overall swelling

Figure 8 shows the relative swelling $R\%$ of CoumSB and SB hydrogels in solutions of targets T3 and T7. In the context of the theory for swelling of ionic hydrogels, the binding of the polyanionic target DNA to the network changes the ionic contribution to the osmotic pressure (T3, T7, T7b), and the concomitant elimination of a crosslink changes the elastic contribution to the osmotic pressure (T3, T7), resulting in gel swelling. The actual relative swelling data (**Figure 8**) reveal a substantial variation in the rate and relative swelling at equilibrium among the independently prepared hydrogels. Despite this variation, which is elaborated below, a clear systematic difference in the initial swelling rate for the different toehold lengths are evident for SBF hydrogels (**Figure 8**c). The mean value of initial swelling rate is 5.3 nm/s for the swelling induced by 20 μM of T3 DNA, which is increased to 25.5 nm/s for the T7 DNA at the same concentration. For SB hydrogels there seems to be some indication of a larger initial swelling rate for T7 than T3, but not as large difference as for the SBF type hydrogels. This could, however, be due to limited number of parallel experiments combined with the rather large observed variations between parallelly prepared hydrogels. Furthermore, a possible impact of different purification method used by the oligonucleotide manufacturer for B strands and fluorescently labelled B strands on the swelling behavior is difficult to assess.

Nevertheless, the difference in the swelling rates between the two toehold lengths, from SBF data as well as from the limited available SB data, is far less than estimates based on the binding rates in solution would suggest. The rate of toehold-mediated strand displacement in solution has been shown to increase exponentially with the toehold length for toeholds up to 7 nucleotides (for toeholds longer than 7, the rate constant reaches a plateau). [39,48] For toehold lengths between 0 and 7 nucleotides, the rate of strand displacement is in order of $10^{toehold}$ $M^{-1}s^{-1}$. As a consequence, if the free target was available to the whole volume of the hydrogel immediately, target T7 binding should be leading to a swelling at a rate 10 000 times greater than T3 binding. From the plot of the swelling degree in **Figure 8**, we can see that this is not the case and the changes in the swelling rate due to the differing toehold lengths are at best moderate.

Effect of toehold length on the migration of the target

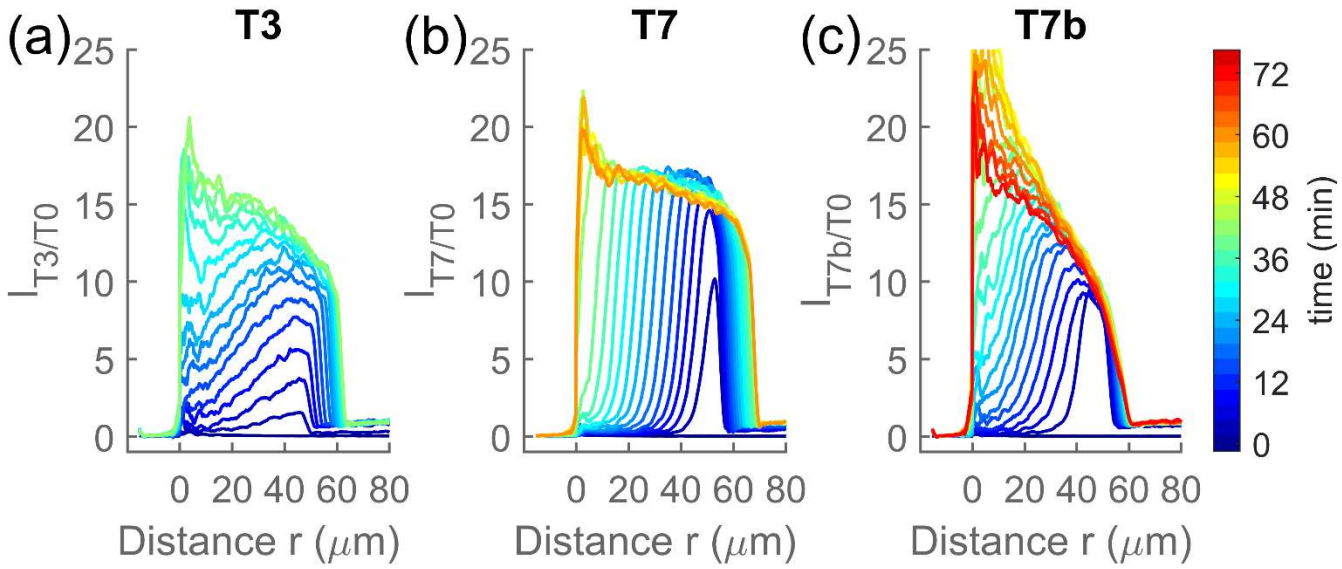

Figure 9 Example of spatiotemporal evolution of relative concentration of the target strand (a) T3, (b) T7 and (c) T7b inside CoumSB hydrogels. A profile is plotted for every 3rd minute. The fiber end faces are located at r = 0.

The overall swelling of the DNA-co-acrylamide hydrogels is the result of a complex interplay in the cascade of processes involving diffusion of the target DNA, its initial binding and toehold-mediated strand displacement. The spatiotemporal relative concentration profiles of target DNA (T3, T7, T7b) represent the sum of concentrations of the free target (T) and the bound target (in SBT or ST) within the hydrogel, and the free target (T) in the surrounding solution. Examples of relative concentration profiles are shown in Figure 9. The profiles show the relative spatiotemporal concentrations of the three different binding targets T3, T7 and T7b in CoumSB hydrogels. The profiles for other parallel preparations of CoumSB hydrogels as well as SB and SBF hydrogels are qualitatively similar (Figure S4, S5 and S6), with the only difference being time to reach equilibrium (with SBF being the slowest on average and SB fastest).

In the case of all three target strands, the target's concentration within the hydrogel is rapidly increasing to levels higher than those in the surrounding solution due to the binding of the target to the DNA conjugated to the network. The maximum equilibrium fluorescence intensity indicates a DNA probe concentration inside the hydrogel from 10 to 25 times the concentration of the surrounding solution. The displacement of the outer edge of the profiles towards increasing *r* reflects the hydrogel swelling.

Notably, the following differences in spatiotemporal concentration profiles of the target DNA reflect the molecular properties of the target DNAs. T3 DNA, with a toehold length of 3 nucleotides, is found to imbibe the DNA-co-AAm hydrogel by gradually increasing its fluorescence intensity throughout the hydrogel. For the particular hydrogel in Figure 9a, already after the first 3 minutes, the T3 DNA concentration in the vicinity of the fiber is reaching the levels of the outside solution. The T3 strand concentration at the hydrogel-solution interface is increasing gradually, reaching its maximum after 18 minutes. In contrast, the T7 DNA (example shown in Figure 9b) is first reaching its maximum concentration on the edge of the hydrogel, already within the first 6 minutes, before any of the target molecules reach the fiber end face. It exhibits a steep wavefront which then moves with unchanged slope of the invading front towards the optical fiber. The target T7b, which has the same toehold as T7, but is not complementary to S on the blocking region, only binds and does not lead to crosslink opening. The concentration profiles of T7b are similar to those of T7, but we observe an increase in fluorescence close to the fiber and a decrease on the outer edge of the hydrogel.

The abrupt peaks in fluorescence observed near the fiber end face (0 – 10 μm), as best seen in Figure 9b, are due to noise introduced by the procedure used to correct for the presence of the fiber. The method is sensitive to misalignments in the radial position of the sample (I_T) and the

reference (I_{T0}).[37] However, an increase in fluorescence intensity beyond this effect has been observed for T7b consistently for all types of hydrogels (Figure 9c and S3-S5). This behavior suggests the presence of a mechanism other than binding and crosslink opening, but at present of unclear origin, which is affecting the partition and/or diffusion of target T7b.

Figure 10 depicts the relative position of the wavefront midpoint in the hydrogel and the slope of the profiles at wavefront midpoint as a function of time for repeated experiments exposing hydrogels SB, CoumSB, and SBF to target strands T3 or T7. The substantial variability in the wavefront movement observed for independently prepared hydrogels can mask differences arising from differing toehold lengths. The wavefront midpoint is seen to invade into SB hydrogels on average faster than in the other hydrogels, with SBF hydrogels being on average the slowest. However, there is a large overlap between, and a large variability within the three hydrogel groups, complicating any conclusions.

The difference in the apparent target diffusion depending on the molecular properties of the toehold is more evident in the slope at the wavefront midpoint (Figure 10). The slopes of wavefronts for apparent T7 diffusion are larger than those for T3 by several orders of magnitude. We can also observe that the slopes of T7 concentration wavefront are nearly constant with time, showing no diffusional broadening. For T3, the wavefront slopes are getting steeper with time as the concentration in the outermost part is increasing faster than at the fiber end face, thus increasing the height of the wavefront and its slope with it. For T3 the slope begins to decrease when the wavefront is reaching the fiber.

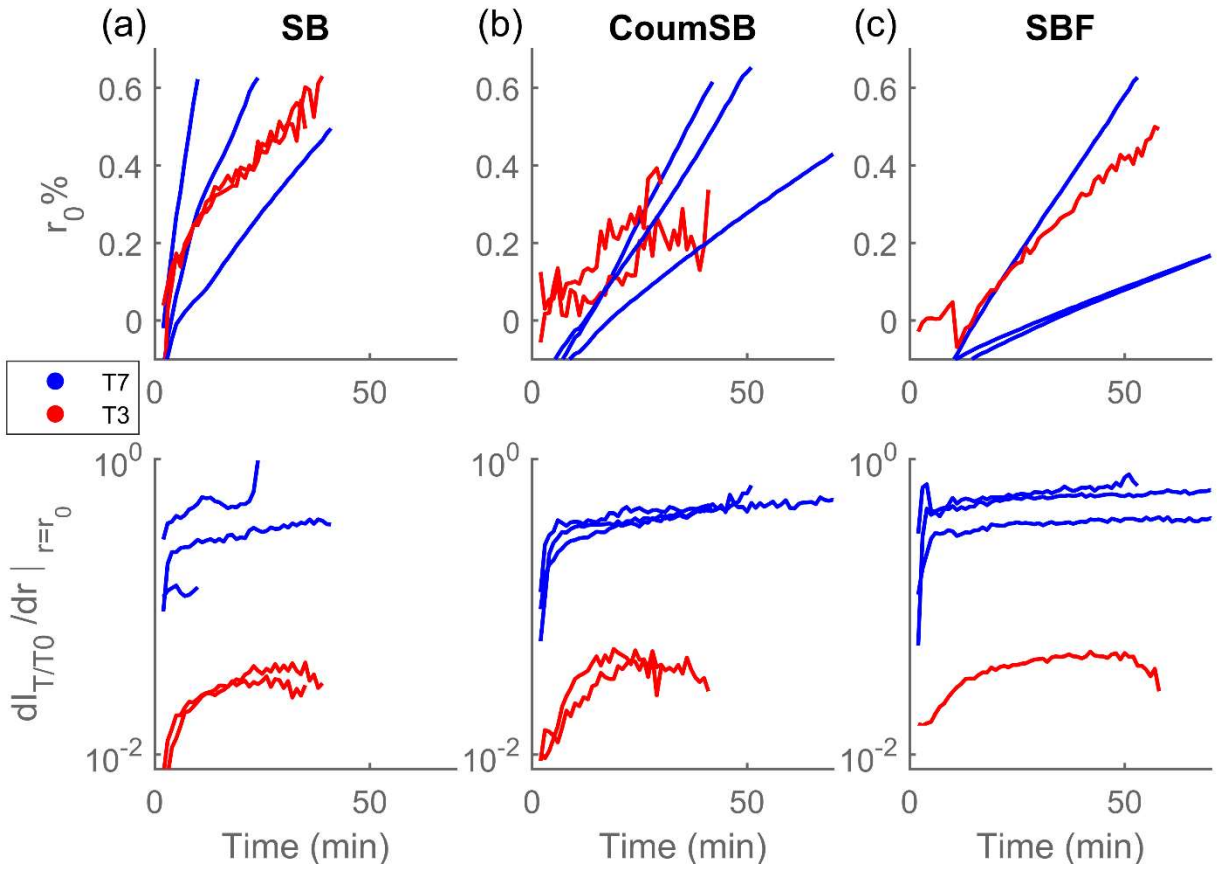

Figure 10 Empirical parameters reflecting the spatiotemporal evolution of the target DNA (T3 and T7) in (a) SB, (b) CoumSB and (c) SBF hydrogels, as deduced from the time-lapse confocal micrographs. These data are the relative position of the wavefront midpoint in the hydrogel r_0% and the slope at the wavefront midpoint. Both shown as a function of time after the targets T3 or T7 where introduced into the solution surrounding the hydrogels at t=0.

Similar to the relative swelling (as determined by interferometry, Figure 8) the time evolution of the wavefront midpoint position r_0% varies between hydrogels and the inter-hydrogel variability in this case seems to mask the difference arising from the different toehold lengths (Figure 10). Possible differences in the heterogeneity among the independently prepared hydrogels, as elaborated below in the context of the parameters obtained using the reaction diffusion modelling, could contribute to the variability.

The longer toehold T7, despite its 10 000 times larger rate of toehold-mediated strand displacement compared to that of T3, offers only a moderate increase in the overall swelling rate of the hydrogel. Qualitative evaluation of the concentration profiles in Figure 9 as well as the values of the slope at wavefront midpoint (Figure 10) offer an explanation. The rate of initial binding of T7 is so high that each hydrogel layer must be filled up to an equilibrium before the target strands can diffuse further without being drained from the diffusable pool by binding to the dsDNA, thus resulting in a sharp front. This is in contrast to a less stable binding of the T3 DNA due to the initial binding to the short toehold being less stable. Targets T3 are detaching from the binding sites on S at a much higher rate and are allowed to diffuse further into the gel between each binding event and the wavefronts are shallower. A similar observation was made for adsorption of various transported proteins in agarose gels by Emily Schirmer and Giorgio Carta.[49] This difference in the effective diffusion has an effect on the overall swelling of the hydrogel. Longer toehold and higher rate of toehold-mediated strand displacement means that although the target is binding stronger and reaching high concentration within the hydrogel very quickly, the binding is occurring in a limited volume compared to the binding of a target with a shorter toehold and consequently the swelling is locally limited to this volume.

Diffusion coefficient and binding rates estimated from reaction-diffusion modelling

Figure 11 shows the same experimental profiles for T3 and T7 in CoumSB hydrogels as were shown in Figure 9, here overlayed with the profiles obtained from the fitting of the reaction-diffusion model (shown for every 3rd minute, but fitting was conducted based on data acquired every minute).

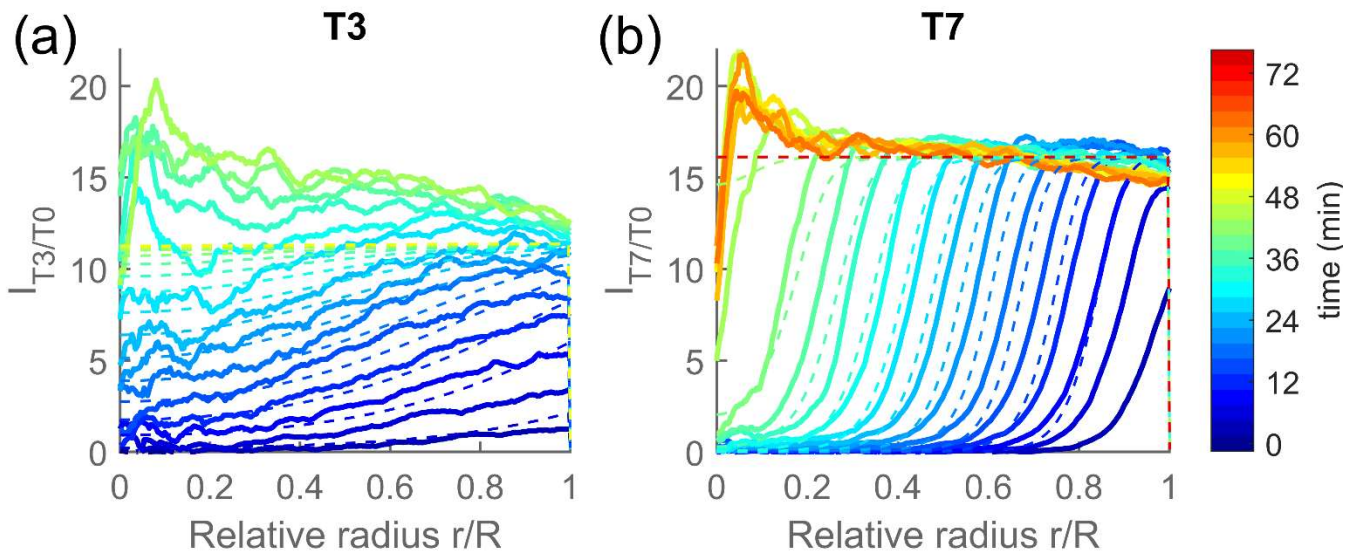

Figure 11 Spatiotemporal evolution of the relative concentration of targets (a) T3 and (b) T7 inside the same CoumSB hydrogels as shown in Figure 9. A profile is plotted for every 3rd minute. In dotted lines, the profiles obtained by fitting the numerical reaction-diffusion model to the experimental data are shown.

Figure 12 depicts the parameters obtained by fitting the reaction-diffusion model to the time evolution of the T3 and T7 target concentration profiles. The parameters estimated this way are the diffusion coefficient *D*, the rate constants, the concentration of available binding sites and a delay parameter that reflects the initiation time for exposing the hydrogels to the aqueous solution with the target DNA. The fitted profiles for the rest of the hydrogels are shown in Figures S7, S8 and S9.

The model fits the T7 profiles better than T3 profiles, but the fits to the reaction-diffusion pattern for both toehold lengths reproduce essential experimentally determined trends. In case of hydrogels exposed to T3, the optimization yielded local minima depending on the starting conditions, where different combinations of rate constants yielded equally adequate fitting curves, while the other parameters were largely unaffected. For reaction rate constants reported

here, the estimates derived from the strand displacement model of Zhang and Winfree[39] were used as starting parameters.

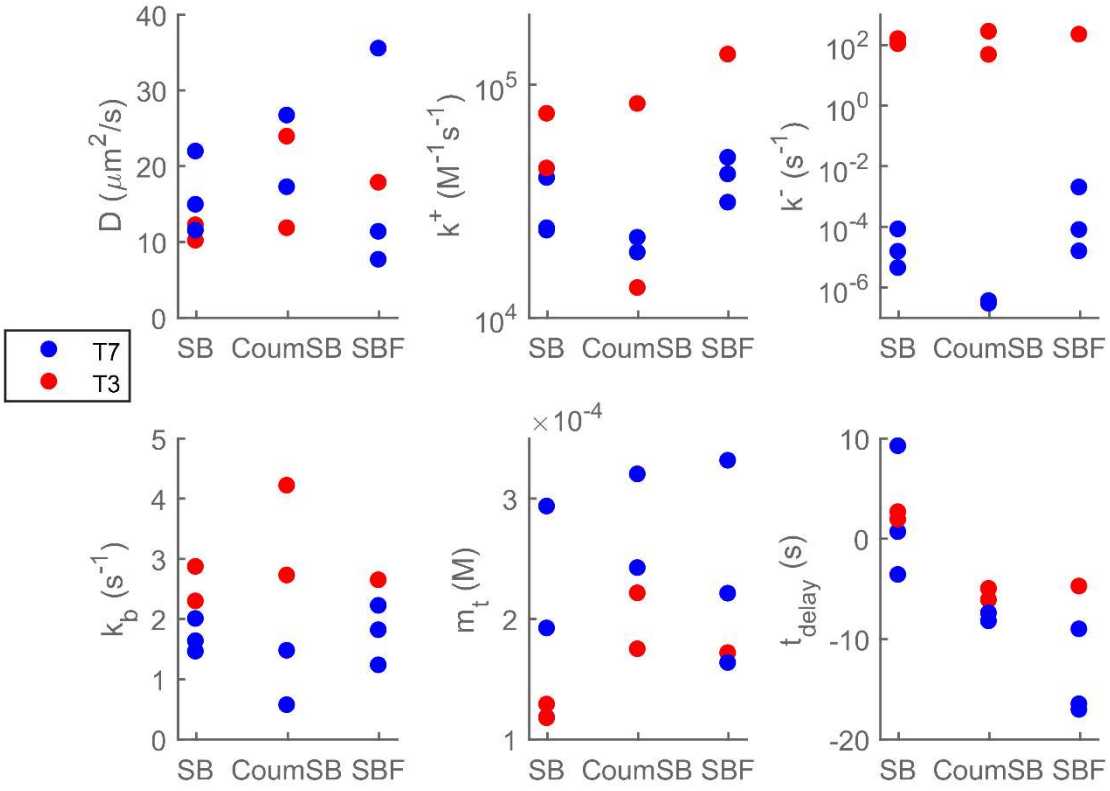

Figure 12 Parameters acquired by fitting experimentally determined reaction-diffusion profiles of the T3 (red symbols) and T7 (blue symbols) target DNA to the reaction-diffusion numerical model for SB, CoumSB and SBF hydrogels when immersed in 20 μM of the target DNA.

An important assumption made when performing the model fitting was that the ratio of the fluorescence intensities between the hydrogel and the surrounding solution reflects the actual concentration ratio (after adjusting for the effect of the fiber presence). This assumption was made in the light of the findings about the different partitioning for the different types of

hydrogels and the fact that the observed partitioning for pure polyacrylamide hydrogel was in agreement with the literature. The difference in the different types of hydrogels was then reflected in the choice of boundary conditions, dictated by the partitioning.

The diffusion coefficient of the target DNA was measured to be 17 ± 8 $\mu m^2/s$. The diffusion coefficient of ssDNA with a number of nucleotides $N \geq 10$ in aqueous solution at 20°C can be estimated by:[52]

$$D_{ssDNA} = 7.38 \text{ x } 10^{-6} N^{-0.539} \text{cm}^2/\text{s}, \quad 31$$

which for a strand of 18 bases leads to $D_{ssDNA,18} = 155\ \mu m^2/s$. The diffusion coefficient is reduced inside the hydrogel. The estimated reduction according to Park et al[53] can be calculated as:

$$\frac{D_{gel}}{D_{sol}} = exp\left(-3.03\ R_h^{0.59} C^{0.94}\right), \quad 32$$

where R_h is the hydrodynamic radius of the solute in angstrom (approx. 20 Å for ssDNA of length 18 bases) and C (g/mL) is the acrylamide concentration (in our case approximately 0.07 g/mL in a swollen hydrogel). This estimates the diffusion coefficient of the target DNA strands in the hydrogel to be 23% of its value in solution, i.e. 36 $\mu m^2/s$.

For polyethylene glycol of varying molecular weight the diffusion coefficient in neutral polyacrylamide hydrogel of the same volume fraction as the hydrogels presented here (0.06) is reduced to 15% of its value in solution.[54] For our ssDNA (which similarly to polyethylene glycol behaves as a random coil), this would reduce the diffusion coefficient to 23 $\mu m^2/s$. A similar value of approximately 30 $\mu m^2/s$ was reported for ssDNA of corresponding molecular weight in polyacrylamide hydrogels[55] (of somewhat different composition than ours,[56] 6%T, 5%C, compared to our approx. 10%T, 2%C, where %T is the total concentration of monomers and %C is the weight percentage of cross-linker).

The concentration of the SB duplex in the pregel solution is 2.82 mmol/L. After polymerization the gels are equilibrated in buffer and they reach a new swelling equilibrium before the target solution is added. This swelling of the hydrogel reduces the concentration of the SB duplex to approximately 2 mmol/L and subsequent swelling induced by the interaction with target ssDNA will reduce this concentration further. However, the apparent concentration of the binding sites that provides the best model fits is 0.2 ± 0.07 mmol/L, i.e. one tenth of the SB concentration as calculated from the initial concentrations. A possible explanation would be that only a tenth of the SB duplexes within the hydrogel is available for binding of the target strands, the other ones being inaccessible due to constraints created by the hydrogel network. The constraints induced by the Aam network and variation in this could originate from the heterogeneity of such network synthesized in a co-polymerization crosslinking reaction.[57–59] As the local environment surrounding the dsDNA are expected to vary both within a particular hydrogel, variation in average accessible dsDNA for binding target DNA can also be expected to occur among parallel preparations. A variation in this available fraction would also explain the differences between the partitioning values for the different hydrogels at equilibrium as well as differences in the relative swelling at equilibrium as measured by the interferometer (**Figure 8**). Thus, a sensor application using this design would have to implement a calibration for each individual hydrogel to account for the variation arising from network heterogeneity.

Table 1 Estimated average values of reaction rate constants and their standard deviations acquired by fitting experimental data to the reaction-diffusion model for T3 and T7 target DNA. Estimated values using prediction models by Zhang and Winfree[39]

	Experimental value[a)]	Estimated value[39]

k^+ ($M^{-1}s^{-1}$)	T3: $10^{(4.7 \pm 0.4)}$ T7:$10^{(4.5 \pm 0.1)}$	T3: 6 x $10^6 = 10^{6.8}$ T7: 6 x $10^6 = 10^{6.8}$
k^- (s^{-1})	T3: $10^{(2.1 \pm 0.3)}$ T7:$10^{(-5 \pm 1)}$	T3: 224.7 $= 10^{2.3}$ T7: 6.6 x $10^{-6} = 10^{-5.2}$
k_b (s^{-1})	2 ± 1	4

a) The averaged values were obtained based on the estimates of the parameter values determined in the fit of the reaction–diffusion model to experiments in several independently prepared SB, CoumSB and SBF hydrogels (Figure 12) for the T3 and T7 target DNA.

The experimentally obtained values of the rate constants k^+, k^- and k_b are shown in Table 1, along with the theoretical values calculated according to Zhang and Winfree[39]. Except for k^+, all the rate constants are within two standard deviations of the theoretical value, and k^- within one standard deviation. The observed reduction in k^+ (which reflects the toehold hybridization rate) compared to its expected value in solution is in accordance with the previously reported decrease in the melting temperature for DNA incorporated within a polyacrylamide hydrogel.[60] Similar effects have been seen for hybridization of DNA bound to a hard surface.[61–65] Shielding of the binding sites, whether by physical, electrostatic or other effects, is usually stated as the underlying mechanism for the reduction in the hybridization rate.

The values of the t_{delay} parameter vary between -20 and +10 minutes. We expected this parameter to be mostly within 1 minute as it was supposed to account for the delay between exposing the hydrogel to the target solution and the first scan within 20-40 seconds. It is possible that the larger values of t_{delay} reflect the fact that swelling was not taken into account by the model and as a result the numerically calculated profiles offer a worse fit to experiment

especially for the initial profiles. Since SBF hydrogels showed on average the slowest target transport, the time before the profiles were fully established further from the edge was the longest, which is possibly reflected in the largest t_{delay} values for SBF hydrogels.

The parameters obtained by model fitting vary little both within and between the three different types of hydrogels (Figure 12), despite the large variability observed for parallelly prepared hydrogels and the response kinetics being on average different for the different hydrogel types (as seen from the evolution of the wavefront midpoint position $r_0\%$, Figure 10 and from spatiotemporal target concentration profiles (Figures S4-S6)).

This suggests that the model accounts for both the hydrogel variability as well as the effect of the fluorescent dyes that define the different hydrogel types. As discussed above, the inherent inhomogeneity of polyacrylamide hydrogels could be reflected in the concentration of the binding sites – a parameter estimated by model fitting.

The addition of the fluorescent dyes was seen to limit the partitioning of the target compared to unlabeled hydrogels, to a degree dependent on the type of the dye. Simulations by Schuck[66] show that lower partition coefficient can have similar effects on the overall transport in a hydrogel as a lower diffusion coefficient. By measuring the partition coefficient for a non-binding target, we were able to take this into account when modelling and use this value to derive the effective experimental boundary conditions. This allowed us to separate the effect of partitioning from that of diffusion and the remaining parameters are consistent between the different hydrogel types. This finding suggests that fluorescent dyes affect hydrogel kinetics mainly through their effect on the target partitioning.

The good agreement of fitted parameters with the literature suggests that the theoretical values of rate constants based on toehold and binding region lengths can be used to predict the behavior

of DNA-hybrid hydrogels. This is despite the fact that these theoretical values are developed for reactions in solution and there is evidence suggesting that tethering DNA to a surface[61,63–65,67] or inside a hydrogel[60] can have an effect on its hybridization kinetics. However, for an accurate simulation of the target reaction-diffusion process, the total available binding site concentration and the partitioning of the target need to be estimated along with the rate constants.

Conclusion

In the present study, we have found that spatiotemporal evolution of migrating target DNA with different molecular properties in dsDNA-co-acrylamide hydrogels yield insight into the interdependence of the cascading processes that precede the swelling, i.e. transport, binding, cross-link opening and localized swelling. In particular, the data indicate that the more strongly interacting target DNA possessing a longer toehold with the conjugated dsDNA is drained from the migrating target DNA pool, yielding a reaction-diffusion pattern with a steep moving wavefront within the hydrogel. In contrast, the hydrogel is filling more gradually throughout its entire volume for the target DNA that possesses a shorter toehold. A change of toehold length thus leads not only to a change in the binding properties of the target, but it has an effect on its transport throughout the gel as well. The resulting swelling is a result of an interaction between these processes. Both the partitioning and the parameter values from the reaction-diffusion modelling of the process indicate that most of the embedded dsDNA in the hydrogels are sterically hindered from interacting with the target DNA. This facet is suggested to arise from the heterogeneous nature of the hydrogels prepared by co-polymerization – crosslinking strategy. On the other hand the diffusion coefficient and the reaction rate constants of the strand displacement were found to be in good agreement with other reported or theoretical values, suggesting the

possibility to use this simple model and theoretical rate constant values to qualitatively predict the spatiotemporal concentration profiles of the target inside the hydrogel. Overall, the fluorescence-based characterization of the spatiotemporal evolution of the migrating target DNA offer novel insight in the underlying processes eventually leading to target DNA induced swelling of dsDNA-co-acrylamide hydrogels.

ASSOCIATED CONTENT

Supporting Information.

Correcting the intensity profiles for the optical effect caused by the presence of the fiber by using Coumarin labelled acrylamide as internal reference (Figure S1); Use of FRET for monitoring of crosslink opening (text); Decrease in Fluorescein's fluorescence intensity in SBF hydrogels, after exposure of the hydrogel to the target solution (Figure S2); Relative swelling kinetics as determined by interferometry of SBF and SB (Figure S3) Spatio-temoral evolution of relative concentrations of the target T3, T7 and T7b inside SB hydrogels (Figure S4), CoumSB hydrogels (Figure S5) and SBF hydrogels (Figure S6); Profiles obtained by fitting the numerical reaction-diffusion model to the experimental profiles of relative concentration of T3 or T7 in SB hydrogels (Figure S7), CoumSB hydrogels (Figure S8) and SBF hydrogels (Figure S9); (PDF)

AUTHOR INFORMATION

Corresponding Author

*E-mail: bjorn.stokke@ntnu.no

Author Contributions

The manuscript was written through contributions of all authors. All authors have given approval to the final version of the manuscript.

Notes

The authors declare no competing financial interest.

ACKNOWLEDGMENT

This research was supported by the Research Council of Norway (Project no 240299/F20).

REFERENCES

(1) Li, J.; Mo, L.; Lu, C.-H.; Fu, T.; Yang, H.-H.; Tan, W. Functional Nucleic Acid-Based Hydrogels for Bioanalytical and Biomedical Applications. *Chem. Soc. Rev.* **2016**, *45* (5), 1410–1431. https://doi.org/10.1039/c5cs00586h.

(2) Liu, J. Oligonucleotide-Functionalized Hydrogels as Stimuli Responsive Materials and Biosensors. *Soft Matter* **2011**, *7* (15), 6757–6767. https://doi.org/10.1039/C1SM05284E.

(3) Xiong, X.; Wu, C.; Zhou, C.; Zhu, G.; Chen, Z.; Tan, W. Responsive DNA-Based Hydrogels and Their Applications. *Macromol. Rapid Commun.* **2013**, *34* (16), 1271–1283. https://doi.org/10.1002/marc.201300411.

(4) Jonášová, E. P.; Stokke, B. T. Bioresponsive DNA-Co-Polymer Hydrogels for Fabrication of Sensors. *Curr. Opin. Colloid Interface Sci.* **2016**, *26*, 1–8. https://doi.org/10.1016/j.cocis.2016.07.001.

(5) Meng, H. M.; Liu, H.; Kuai, H.; Peng, R.; Mo, L.; Zhang, X. B. Aptamer-Integrated DNA Nanostructures for Biosensing, Bioimaging and Cancer Therapy. *Chem. Soc. Rev.* **2016**, *45* (9), 2583–2602. https://doi.org/10.1039/c5cs00645g.

(6) Aldaye, F. A.; Palmer, A. L.; Sleiman, H. F. Assembling Materials with DNA as the Guide. *Science (80-.).* **2008**, *321* (5897), 1795–1799. https://doi.org/10.1126/science.1154533.

(7) Seeman, N. C. DNA in a Material World. *Nature* **2003**, *421*, 427–431. https://doi.org/10.1038/nature01406.

(8) Roh, Y. H.; Ruiz, R. C. H.; Peng, S.; Lee, J. B.; Luo, D. Engineering DNA-Based Functional Materials. *Chem. Soc. Rev.* **2011**, *40* (12), 5730–5744. https://doi.org/10.1039/c1cs15162b.

(9) Chao, J.; Zhu, D.; Zhang, Y.; Wang, L.; Fan, C. DNA Nanotechnology-Enabled Biosensors. *Biosens. Bioelectron.* **2016**, *76*, 68–79. https://doi.org/10.1016/j.bios.2015.07.007.

(10) Zhang, F.; Nangreave, J.; Liu, Y.; Yan, H. Structural DNA Nanotechnology: State of the Art and Future Perspective. *J. Am. Chem. Soc.* **2014**, *136* (32), 11198–11211. https://doi.org/10.1021/ja505101a.

(11) Pinheiro, A. V.; Han, D.; Shih, W. M.; Yan, H. Challenges and Opportunities for Structural DNA Nanotechnology. *Nature Nanotechnology*. Nature Publishing Group December 6, 2011, pp 763–772. https://doi.org/10.1038/nnano.2011.187.

(12) Mao, Y.; Li, J.; Yan, J.; Ma, Y.; Song, Y.; Tian, T.; Liu, X.; Zhu, Z.; Zhou, L.; Yang, C. A Portable Visual Detection Method Based on a Target-Responsive DNA Hydrogel and Color Change of Gold Nanorods. *Chem. Commun.* **2017**, *53* (47), 6375–6378. https://doi.org/10.1039/c7cc01360d.

(13) Kim, T.; Park, S.; Lee, M.; Baek, S.; Lee, J. B.; Park, N. DNA Hydrogel Microspheres and Their Potential Applications for Protein Delivery and Live Cell Monitoring. *Biomicrofluidics* **2016**, *10* (3). https://doi.org/10.1063/1.4953046.

(14) Ma, Y.; Mao, Y.; An, Y.; Tian, T.; Zhang, H.; Yan, J.; Zhu, Z.; Yang, C. J. Target-Responsive DNA Hydrogel for Non-Enzymatic and Visual Detection of Glucose. *Analyst*

2018, *143*, 1679–1684. https://doi.org/10.1039/c8an00010g.

(15) Liu, S.; Su, W.; Li, Y.; Zhang, L.; Ding, X. Manufacturing of an Electrochemical Biosensing Platform Based on Hybrid DNA Hydrogel: Taking Lung Cancer-Specific MiR-21 as an Example. *Biosens. Bioelectron.* **2018**, *103*, 1–5. https://doi.org/10.1016/j.bios.2017.12.021.

(16) Yang, H.; Liu, H.; Kang, H.; Tan, W. Engineering Target-Responsive Hydrogels Based on Aptamer--Target Interactions. *J. Am. Chem. Soc.* **2008**, *130* (20), 6320–6321. https://doi.org/10.1021/ja801339w.

(17) Srinivas, R. L.; Chapin, S. C.; Doyle, P. S. Aptamer-Functionalized Microgel Particles for Protein Detection. *Anal. Chem.* **2011**, *83* (23), 9138–9145. https://doi.org/10.1021/ac202335u.

(18) Bai, W.; Spivak, D. A. A Double-Imprinted Diffraction-Grating Sensor Based on a Virus-Responsive Super-Aptamer Hydrogel Derived from an Impure Extract. *Angew. Chemie Int. Ed.* **2014**, *53* (8), 2095–2098. https://doi.org/10.1002/anie.201309462.

(19) Wei, X.; Tian, T.; Jia, S.; Zhu, Z.; Ma, Y.; Sun, J.; Lin, Z.; Yang, C. J. Microfluidic Distance Readout Sweet Hydrogel Integrated Paper-Based Analytical Device (MDiSH-PAD) for Visual Quantitative Point-of-Care Testing. *Anal. Chem.* **2016**, *88* (4), 2345–2352. https://doi.org/10.1021/acs.analchem.5b04294.

(20) Joseph, K. A.; Dave, N.; Liu, J. Electrostatically Directed Visual Fluorescence Response of DNA-Functionalized Monolithic Hydrogels for Highly Sensitive Hg2+ Detection. *ACS Appl. Mater. Interfaces* **2011**, *3* (3), 733–739. https://doi.org/10.1021/am101068c.

(21) Ye, B.-F.; Zhao, Y.-J.; Cheng, Y.; Li, T.-T.; Xie, Z.-Y.; Zhao, X.-W.; Gu, Z.-Z. Colorimetric Photonic Hydrogel Aptasensor for the Screening of Heavy Metal Ions. *Nanoscale* **2012**, *4* (19), 5998–6003. https://doi.org/10.1039/c2nr31601c.

(22) Song, P.; Ye, D.; Zuo, X.; Li, J.; Wang, J.; Liu, H.; Hwang, M. T.; Chao, J.; Su, S.; Wang, L. L.; et al. DNA Hydrogel with Aptamer-Toehold-Based Recognition, Cloaking, and Decloaking of Circulating Tumor Cells for Live Cell Analysis. *Nano Lett.* **2017**, *17* (9), 5193–5198. https://doi.org/10.1021/acs.nanolett.7b01006.

(23) Chen, W. H.; Liao, W. C.; Sohn, Y. S.; Fadeev, M.; Cecconello, A.; Nechushtai, R.; Willner, I. Stimuli-Responsive Nucleic Acid-Based Polyacrylamide Hydrogel-Coated Metal–Organic Framework Nanoparticles for Controlled Drug Release. *Adv. Funct. Mater.* **2018**, *28*, 1705137.1-1705137.9. https://doi.org/10.1002/adfm.201705137.

(24) Lai, J.; Li, S.; Shi, X.; Coyne, J.; Zhao, N.; Dong, F.; Mao, Y.; Wang, Y. Displacement and Hybridization Reactions in Aptamer-Functionalized Hydrogels for Biomimetic Protein Release and Signal Transduction. *Chem. Sci.* **2017**, *8* (11), 7306–7311. https://doi.org/10.1039/c7sc03023a.

(25) Wang, Z.; Xia, J.; Cai, F.; Zhang, F.; Yang, M.; Bi, S.; Gui, R.; Li, Y.; Xia, Y. Aptamer-Functionalized Hydrogel as Effective Anti-Cancer Drugs Delivery Agents. *Colloids Surfaces B Biointerfaces* **2015**, *134*, 40–46. https://doi.org/10.1016/j.colsurfb.2015.06.031.

(26) Jiang, F. X.; Yurke, B.; Firestein, B. L.; Langrana, N. A. Neurite Outgrowth on a DNA Crosslinked Hydrogel with Tunable Stiffnesses. *Ann. Biomed. Eng.* **2008**, *36* (9), 1565–

1579. https://doi.org/10.1007/s10439-008-9530-z.

(27) Shao, Y.; Jia, H.; Cao, T.; Liu, D. Supramolecular Hydrogels Based on DNA Self-Assembly. *Acc. Chem. Res.* **2017**, *50* (4), 659–668. https://doi.org/10.1021/acs.accounts.6b00524.

(28) Zhang, Z.; Du, J.; Li, Y.; Wu, J.; Yu, F.; Chen, Y. An Aptamer-Patterned Hydrogel for the Controlled Capture and Release of Proteins: Via Biorthogonal Click Chemistry and DNA Hybridization. *J. Mater. Chem. B* **2017**, *5* (30), 5974–5982. https://doi.org/10.1039/c7tb00883j.

(29) Cangialosi, A.; Yoon, C. K.; Liu, J.; Huang, Q.; Guo, J.; Nguyen, T. D.; Gracias, D. H.; Schulman, R. DNA Sequence–Directed Shape Change of Photopatterned Hydrogels via High-Degree Swelling. *Science (80-.).* **2017**, *357* (6356), 1126–1130. https://doi.org/10.1126/science.aan3925.

(30) Fern, J.; Scalise, D.; Cangialosi, A.; Howie, D.; Potters, L.; Schulman, R. DNA Strand-Displacement Timer Circuits. *ACS Synth. Biol.* **2017**, *6* (2), 190–193. https://doi.org/10.1021/acssynbio.6b00170.

(31) Tierney, S.; Hjelme, D. R.; Stokke, B. T. B. T. Determination of Swelling of Responsive Gels with Nanometer Resolution. Fiber-Optic Based Platform for Hydrogels as Signal Transducers. *Anal. Chem.* **2008**, *80* (13), 5086–5093. https://doi.org/10.1021/ac800292k.

(32) Nagahara, S.; Matsuda, T. Hydrogel Formation via Hybridization of Oligonucleotides Derivatized in Water-Soluble Vinyl Polymers. *Polym. Gels Networks* **1996**, *4* (2), 111–127. https://doi.org/http://dx.doi.org/10.1016/0966-7822(96)00001-9.

(33) Tierney, S.; Stokke, B. T. Development of an Oligonucleotide Functionalized Hydrogel Integrated on a High Resolution Interferometric Readout Platform as a Label-Free Macromolecule Sensing Device. *Biomacromolecules* **2009**, *10* (6), 1619–1626. https://doi.org/10.1021/bm900218c.

(34) Gao, M.; Gawel, K.; Stokke, B. T. Toehold of DsDNA Exchange Affects the Hydrogel Swelling Kinetics of a Polymer-DsDNA Hybrid Hydrogel. *Soft Matter* **2011**, *7* (5), 1741–1746. https://doi.org/10.1039/c0sm00915f.

(35) Kibbe, W. A. (Northwestern U. OligoCalc: An Online Oligonucleotide Properties Calculator. *Nucleic Acids Research*. 2007. https://doi.org/10.1093/nar/gkm234.

(36) Gehrke, S. H.; Fisher, J. P.; Palasis, M.; Lund, M. E. Factors Determining Hydrogel Permeability. *Ann. N. Y. Acad. Sci.* **2006**, *831* (1), 179–184. https://doi.org/10.1111/j.1749-6632.1997.tb52194.x.

(37) Jonášová, E. P.; Bjørkøy, A.; Stokke, B. T. Recovering Fluorophore Concentration Profiles from Confocal Images near Lateral Refractive Index Step Changes. *J. Biomed. Opt.* **2016**, *21* (12), 126014. https://doi.org/10.1117/1.JBO.21.12.126014.

(38) Ford Versypt, A. N.; Arendt, P. D.; Pack, D. W.; Braatz, R. D. Derivation of an Analytical Solution to a Reaction-Diffusion Model for Autocatalytic Degradation and Erosion in Polymer Microspheres. *PLoS One* **2015**, *10* (8), e0135506.1-e0135506.14. https://doi.org/10.1371/journal.pone.0135506.

(39) Zhang, D. Y.; Winfree, E. Control of DNA Strand Displacement Kinetics Using Toehold Exchange. *J. Am. Chem. Soc.* **2009**, *131* (47), 17303–17314.

(40) Yurke, B.; Mills, A. P. Using DNA to Power Nanostructures. *Genet. Program. Evolvable Mach.* **2003**, *4* (2), 111–122. https://doi.org/10.1023/A:1023928811651.

(41) Crank, J. The Mathematics of Diffusion. In *Clarendon Press*; Oxford University Press: Oxford, 1975; pp 148–149.

(42) Ogston, A. G. The Spaces in a Uniform Random Suspension of Fibres. *Trans. Faraday Soc.* **1958**, *54* (0), 1754–1757. https://doi.org/10.1039/TF9585401754.

(43) Sim, A. Y. L.; Lipfert, J.; Herschlag, D.; Doniach, S. Salt Dependence of the Radius of Gyration and Flexibility of Single-Stranded DNA in Solution Probed by Small-Angle x-Ray Scattering. *Phys. Rev. E* **2012**, *86*, 021901.1-021901.5.

(44) Williams Jr, J. C.; Mark, L. A.; Eichholtz, S.; Williams, J. C.; Mark, L. A.; Eichholtz, S. Partition and Permeation of Dextran in Polyacrylamide Gel. *Biophys. J.* **1998**, *75* (1), 493–502. https://doi.org/http://dx.doi.org/10.1016/S0006-3495(98)77538-1.

(45) Dannenfelser, R. M.; Yalkowsky, S. H. Data Base of Aqueous Solubility for Organic Non-Electrolytes. *Sci. Total Environ.* **1991**, *109–110* (C), 625–628.

(46) Dehn, W. M. Comparative Solubilities in Water, in Pyridine and in Aqueous Pyridine. *J. Am. Chem. Soc.* **1917**, *39* (7), 1399–1404. https://doi.org/10.1021/ja02252a012.

(47) Yamada, A.; Hiruta, Y.; Wang, J.; Ayano, E.; Kanazawa, H. Design of Environmentally Responsive Fluorescent Polymer Probes for Cellular Imaging. *Biomacromolecules* **2015**, *16* (8), 2356–2362. https://doi.org/10.1021/acs.biomac.5b00591.

(48) Li, Q.; Luan, G.; Guo, Q.; Liang, J. A New Class of Homogeneous Nucleic Acid Probes

Based on Specific Displacement Hybridization. *Nucleic Acids Res.* **2002**, *30* (2), e5–e5.

(49) Schirmer, E. B.; Carta, G. Protein Adsorption in Charged Agarose Gels Studied by Light Microscopy. *AIChE J.* **2007**, *53* (6), 1472–1482. https://doi.org/10.1002/aic.11191.

(50) Sjöback, R.; Nygren, J.; Kubista, M. Characterization of Fluorescein – Oligonucleotide Conjugates and Measurement of Local Electrostatic Potential. *Biopolymers* **1998**, *46*, 445–453.

(51) Moreira, B. G.; You, Y.; Behlke, M. A.; Owczarzy, R. Effects of Fluorescent Dyes, Quenchers, and Dangling Ends on DNA Duplex Stability. *Biochem. Biophys. Res. Commun.* **2005**, *327* (2), 473–484.

(52) Stellwagen, E.; Lu, Y.; Stellwagen, N. C. Unified Description of Electrophoresis and Diffusion for DNA and Other Polyions. *Biochemistry* **2003**, *42* (40), 11745–11750.

(53) Park, I. H.; Johnson, C. S.; Hill, C.; Carolina, N.; Gabriel, D. A. Probe Diffusion in Polyacrylamide Gels. *Macromolecules* **1990**, *21*, 1548–1553.

(54) Tong, J.; Anderson, J. L. Partitioning and Diffusion of Proteins and Linear Polymers in Polyacrylamide Gels. *Biophys. J.* **1996**, *70* (3), 1505–1513.

(55) Yin, H.; Kleemiß, M. H.; Lux, J. A.; Schomburg, G. Diffusion Coefficients of Oligonucleotides in Capillary Gel Electrophoresis. *J. Microcolumn Sep.* **1991**, *3* (4), 331–335. https://doi.org/10.1002/mcs.1220030407.

(56) Yin, H.; Lux, J. A.; Schomburg, G. Production of Polyacrylamide Gel Filled Capillaries for Capillary Gel Electrophoresis (CGE): Influence of Capillary Surface Pretreatment on

Performance and Stability. *J. High Resolut. Chromatogr.* **1990**, *13* (9), 624–627. https://doi.org/10.1002/jhrc.1240130908.

(57) Shibayama, M. Universality and Specificity of Polymer Gels Viewed by Scattering Methods. *Bull. Chem. Soc. Jpn.* **2006**, *79* (12), 1799–1819. https://doi.org/10.1246/bcsj.79.1799.

(58) Habicht, A.; Schmolke, W.; Lange, F.; Saalwächter, K.; Seiffert, S. The Non-Effect of Polymer-Network Inhomogeneities in Microgel Volume Phase Transitions: Support for the Mean-Field Perspective. *Macromol. Chem. Phys.* **2014**, *215* (11), 1116–1133. https://doi.org/10.1002/macp.201400114.

(59) Di Lorenzo, F.; Seiffert, S. Nanostructural Heterogeneity in Polymer Networks and Gels. *Polym. Chem.* **2015**, *6* (31), 5515–5528. https://doi.org/10.1039/c4py01677g.

(60) Fotin, A. V.; Drobyshev, A. L.; Proudnikov, D. Y.; Perov, A. N.; Mirzabekov, A. D. Parallel Thermodynamic Analysis of Duplexes on Oligodeoxyribonucleotide Microchips. *Nucleic Acids Res.* **1998**, *26* (6), 1515–1521.

(61) Hoefert, M. J.; Sambriski, E. J.; de Pablo, J. J. Molecular Pathways in DNA-DNA Hybridization of Surface-Bound Oligonucleotides. *Soft Matter* **2011**, *7*, 560–566.

(62) Wong, I. Y.; Melosh, N. A. An Electrostatic Model for DNA Surface Hybridization. *Biophys. J.* **2010**, *98* (12), 2954–2963.

(63) Hagan, M. F.; Chakraborty, A. K. Hybridization Dynamics of Surface Immobilized DNA. *J. Chem. Phys.* **2004**, *120* (10), 4958–4968.

(64) Peterson, A. W.; Heaton, R. J.; Georgiadis, R. M. The Effect of Surface Probe Density on DNA Hybridization. *Nucleic Acids Res.* **2001**, *29* (24), 5163–5168.

(65) Vainrub, A.; Pettitt, B. M. Accurate Prediction of Binding Thermodynamics for DNA on Surfaces. *J. Phys. Chem. B* **2011**, *115* (45), 13300–13303.

(66) Schuck, P. Kinetics of Ligand Binding to Receptor Immobilized in a Polymer Matrix, as Detected with an Evanescent Wave Biosensor. I. A Computer Simulation of the Influence of Mass Transport. *Biophys. J.* **1996**, *70* (3), 1230–1249. https://doi.org/http://dx.doi.org/10.1016/S0006-3495(96)79681-9.

(67) Erickson, D.; Li, D.; Krull, U. J. Modeling of DNA Hybridization Kinetics for Spatially Resolved Biochips. *Anal. Biochem.* **2003**, *317* (2), 186–200.

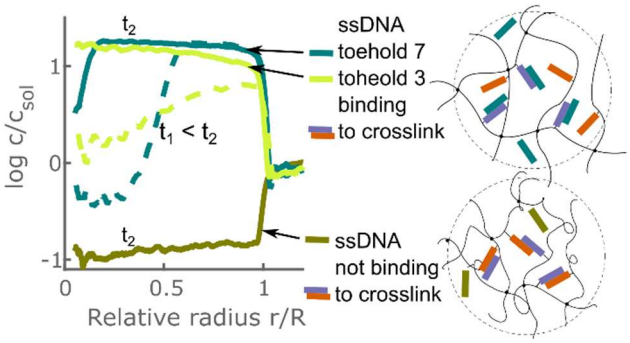

Figure 13 For Table of Contents only